

Report for the Joint Use/Research of the Institute for Planetary Materials, Okayama University for FY2024

Month 5/Day 31/Year 2025

Category: International Joint Research General Joint Research Joint Use of Facility
Workshop

Name of the research project: The synergistic effect of temperature and pressure on the graphitization of individual maceral and the kinetic model of graphitization

Principal applicant: Wang Yuhui

Affiliated institution and department: Nanjing University, School of Earth Sciences and Engineering, State Key Laboratory for Mineral Deposits Research

Collaborator

Name: Takashi Yoshino

Affiliated institution and department: Institute for Planetary Materials, Okayama University

Research report:

1. Research Background

The widespread application and rapid development of carbon materials provide a broad prospect for the efficient and comprehensive utilization of coal. Since the discovery of fullerene and onion carbon in sub-graphite, ultra-anthracite, and thermally metamorphosed coal in 1992 and 2000 (Buseck et al., 1992; Atul et al., 2000), many naturally formed carbon nanostructures have been found in natural coal, especially in the high metamorphic anthracite-graphite stage (Yilin Chen et al., 2022). Therefore, carbon nanomaterials existing in natural coal have broad development prospects. As natural carbon nanomaterials often form in the high metamorphic anthracite-graphite stage, studying the process and formation mechanism of coal graphitization can help deepen the understanding of the formation process of natural carbon materials and their potential applications.

There are many factors influencing the graphitization of coal, including temperature, pressure, shear strain, and hydrothermal fluid activity, all of which have a significant impact on the graphitization process (Bustin et al., 1995; Ross and Bustin, 1990; Wilks et al., 1993; Suchy et al., 1997; Rantitsch et al., 2004). Studies have pointed out that under the action of temperature alone, complete graphitization only occurs at temperatures above 2000°C (Oberlin, 1984). Bonijoly and others (1982) believe that under the action of temperature alone, organic matter is difficult to graphitize, and pressure and shear stress play a very important role in the formation

of graphite. Coal-based graphite is formed by coal and coal-based carbonaceous shale under the action of magma contact metamorphism and structural metamorphism (Cao et al., 2017, 2020), indicating that pressure is an important factor in carbon transformation. Suchy and others (1997) found that frictional heat is the main factor for the structural transformation of organic matter in shear zones to form autogenous graphite. The huge static pressure of the stratum is conducive to the regular arrangement of aromatic ring clusters on parallel planes (Beysac et al., 2002), so high pressure will accelerate the graphitization process of organic matter (Nover et al., 2005). High temperature and high pressure experiments show that stress will cause the disorderly distributed aromatic carbon precursors to connect with each other, arrange in an oriented manner, increase the order, and small strain rates and large deformations are conducive to the growth of the basic structural units La and Lc of coal (Nover et al., 2005). Therefore, it is believed that a large amount of graphite produced in thrust faults and overthrust bodies is caused by structural stress, and high pressure will accelerate the graphitization process of organic matter (Jiang et al., 2016). The most important thing is that there is a clear temperature-pressure synergy in coal graphitization. The influence of pressure on the graphitization process has both positive and negative effects, which are greatly related to temperature: temperature and pressure synergy will promote the orientation and bonding of aromatic layers, playing a positive role in the graphitization process; temperature and pressure imbalance, high pressure will disassemble the aromatic layers, playing a negative role in the graphitization process (Liu, 2021). However, there is currently a lack of research on quantifying the temperature-pressure coupling effect, leading to an incomplete understanding of the impact and mechanism of temperature-pressure synergy on coal graphitization.

In contrast, carbonaceous materials (CM) represent ubiquitous accessory phases in sedimentary environments, undergoing dynamic changes in composition and structure during metamorphic processes (Buseck and Beysac, 2014). The transition of CM to graphite serves as a pivotal geothermometer in geologic settings characterized by low to moderate metamorphic temperatures, thereby serving as a widely utilized tool for geothermal assessment (Beysac et al., 2002; Kouketsu et al., 2014). However, this transformation is not merely a simple recrystallization process solely dependent on metamorphic temperature. As previously mentioned, the evolution of organic precursors in CM is influenced by the combined effects of temperature and pressure on chemical composition, microstructure, and crystallinity. The multifaceted changes occurring during the conversion from organic matter to graphite pose challenges for the understanding of natural CM structures, with comprehensive evaluations of these factors during graphitization processes being infrequently achieved. Therefore, the adoption of a fundamental kinetic model becomes imperative to elucidate the natural graphitization processes at geological time scales and crustal temperatures. Research on the kinetics of graphitization remains limited within academic discourse. A significant barrier to synthetic graphite production lies in the necessity for extremely high processing temperatures (~3000 K) and low fO_2 environments. Early kinetic investigations in the 1960s to early 1970s estimated an effective activation energy for graphite formation to be around 1000 kJ/mol (e.g., Fischbach, 1963, 1971; Murty et al., 1969), consistent with vacancy diffusion experiments utilizing natural graphite (Kanter, 1957) and first-principles calculations (Kaxiras &

Pandey, 1988). However, markedly high effective activation energies in experimental data underscore significant disparities between the natural and experimental trajectories of carbonaceous material structural evolution. Inferences based on previous experimental kinetic data at 1 atmosphere suggest that even at 700°C, graphite synthesis would necessitate approximately 1040 minutes (approximately 1.9×10^{34} years; Fischbach, 1971; Bustin et al., 1995). Therefore, we need to provide more realistic experimental kinetic models and more realistically constrained experimental data to understand the temperature-pressure synergy and the underlying kinetics of coal graphitization.

Previous investigations into the synthesis of graphite have highlighted the significant influence of precursor material nanostructure on the structural transition of carbonaceous materials (CM) to graphite (Oberlin 1984; Oberlin et al. 2006). Coal, as a widely distributed organic rock in nature, comprises diverse types of sedimentary organic matter (maceral). Coal has a complex composition, primarily divided into mineral matter (ash) and macerals. The macerals can be classified into Type I, II, and III according to organic petrology (Tissot et al., 1980), each exhibiting distinct physical properties and chemical compositions leading to divergent physiochemical evolution pathways (Huang et al., 1995; Yao et al., 1996; Chen et al., 1999). The intricate interplay of diverse mechanisms resultant from disparate maceral constituents complicates and enriches the graphitization trajectory of coal, thus impeding the attainment of a unified comprehension of coal graphitization. Regrettably, previous investigations into coal graphitization and its kinetics have frequently disregarded the pivotal role of organic matter typologies. While various macerals form the fundamental building blocks of coal, research elucidating their individual impacts on graphitization remains scant, thereby obstructing the delineation of coal graphitization patterns and kinetic models. Through the meticulous isolation and enrichment of distinct macerals from coal samples, coupled with high-temperature and high-pressure graphitization experiments conducted on these segregated macerals, we can effectively surmount the intricacies inherent in coal evolution stemming from compositional heterogeneity. This endeavor significantly contributes to unraveling the synergistic effects of temperature and pressure in the coal graphitization process, facilitating the refinement of natural graphitization kinetic models. Consequently, our enhanced understanding of graphitization dynamics within natural contexts spanning geological timescales not only fosters theoretical advancements but also furnishes a substantive framework for the synthesis of coal-derived carbon materials.

2. Research content

2.1 Investigation of the microstructural evolution patterns of individual macerals under varying thermal and pressure conditions

Utilizing optical microscopy, high-resolution transmission electron microscopy (HRTEM), EBSD-SEM, and XRD techniques, our study aims to observe and analyze samples (solid residues) from temperature and pressure-controlled simulated experiments at both micro and nanoscopic levels. This endeavor aims to unveil the micro and nanoscale structures of macerals under different pressure conditions, elucidating the variations and evolutionary patterns in aggregated molecular structures. Our objective is to investigate the fracture and reconfiguration processes of molecular structures of macerals under pressure, revealing the evolutionary

mechanisms of different macerals macromolecular structures under pressure.

2.2 Establishment of graphitization kinetic model for single macerals

By employing X-ray diffraction (XRD) and Raman spectroscopy techniques, we aim to elucidate the correlations between changes in crystallinity, morphology, and nanoscale structures with the duration and conditions of processing. We anticipate the utilization of power law models (Murty et al., 1969), Johnson-Mehl-Avrami (JMA) models (Sung, 2000; Khawam and Flanagan, 2006), and superimposition methods (Fischbach, 1963; Inagaki et al., 1968) to construct a comprehensive graphitization kinetic model. This endeavor aims to shed light on the natural graphitization processes under geological time scales and crustal temperatures, providing crucial insights for establishing models on the synergistic effects of temperature and pressure on coal thermal evolution.

2.3 Establishment of a model for the thermal-pressure synergistic effects on coal graphitization

In light of the insights gleaned from the preceding investigations, we amalgamate the structural evolution and kinetic models pertinent to the high-temperature, high-pressure graphitization process of coal macerals. Our endeavor situates this amalgamation within the geological milieu of tectonic metamorphic zones, with the overarching objective of formulating a comprehensive framework that accounts for the synergistic interplay between temperature and pressure in coal graphitization phenomena. The resultant model aspires to furnish a robust theoretical foundation conducive to the delineation of strategies for graphite exploration and the synthesis of carbon nanomaterials derived from coal reserves.

3. Experimental methods

3.1 Sample Preparation and Micro-component Separation

First, we will collect typical low-maturity coal samples that are rich in single maceral. Based on our previous research, we will mainly collect special coal samples for shell-rich samples, including Leping bark liptobiolith (for extracting barkinite), and HunYuan Boghead coal (for extracting inextinite). For vitrinite-rich samples, we will mainly collect Jurassic coal from the Ordos Basin. Maceral will be enriched through a combination of hand-picking and heavy liquid separation. The heavy liquid separation method has a good effect on the enrichment of macerals and has been used by many researchers. Therefore, this study will use sodium polytungstate heavy liquid density gradient centrifugation method to enrich macerals. The enriched purity of the macerals, which will be checked under a microscope and used as simulation experiment samples, should reach over 98% for vitrinite and barkinite, and over 95% for inextinite.

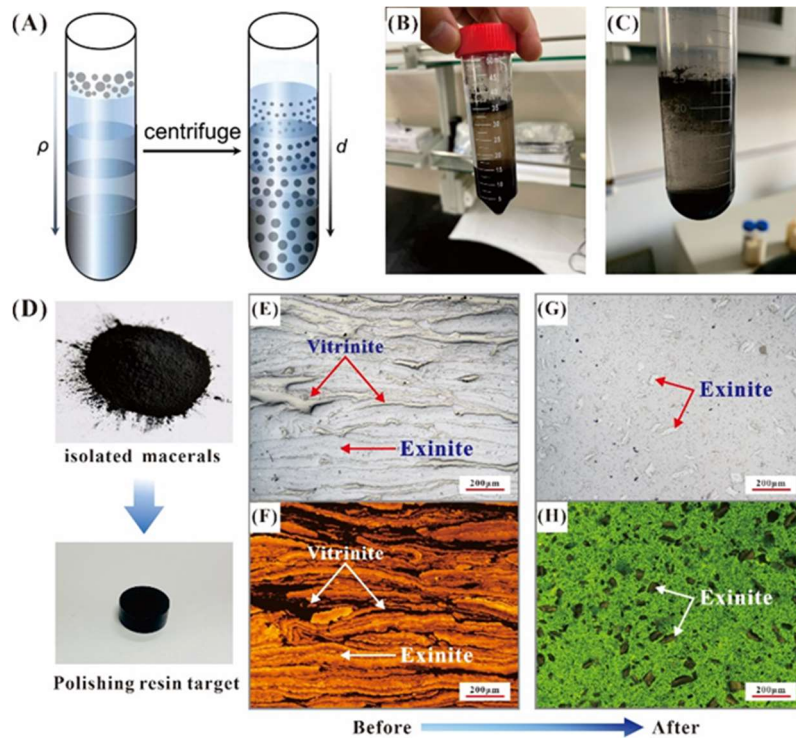


Figure 1. Maceral enrichment and separation schematic diagram

Note that we have completed this part of the sample preparation in Nanjing University.

2.2 High Temperature and High Pressure Controlled Simulation Experiments

We plan to conduct high-temperature and high-pressure simulation experiments on vitrinite, barkinite, alginate and sporinite. The experiments will mainly be conducted through a multi anvil apparatus (piston-cylinder apparatus or Kawai-type apparatus).

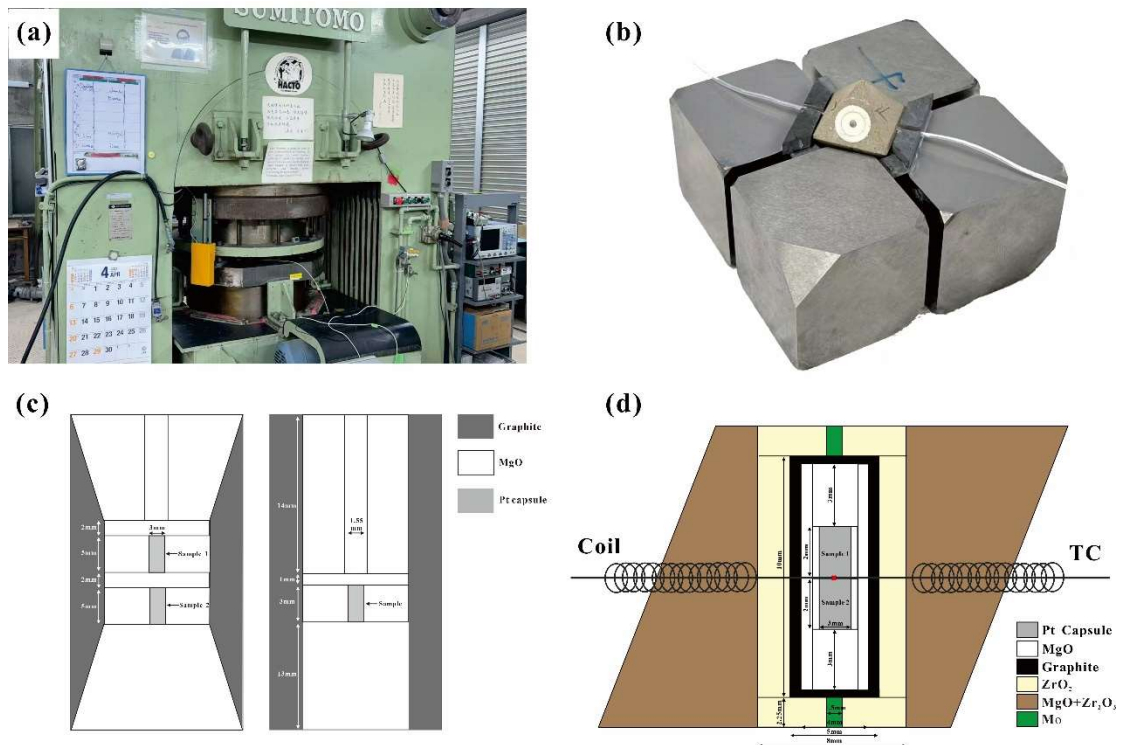


Figure 2. Schematic illustration of the high-pressure cell assemblage used for experiments. (a) multi-anvil

apparatus; (b) Actual assembly photo of Kawai-type press 18/11; (c) Schematic diagram of 3/4 and 1/2 scale piston-cylinder press assembly; (d) Schematic diagram of Kawai-type press 18/11 assembly.

The Multi anvil apparatus experiment involves a larger sample size and is mainly used for the study of the temperature and pressure synergy and kinetic process of organic matter graphitization. We have already conducted some experiments and have obtained some good research results. We have used a piston-cylinder press to conduct a series of high-temperature and high-pressure experiments (500MPa, 700MPa, 900MPa, 1GPa, 2GPa, and 3GPa, 800°C) on hydrogen-rich barkinite and oxygen-rich vitrinite. The experimental reaction time is 24 hours, and the annealing rate is 100°C/minute. In order to achieve the planned kinetic research, we will control the annealing time to be 10min, 60min, 360min, 720min, 1440min, and will conduct a 1s short-time quench for comparison. The heating rate is controlled at 100°C/minute, and the temperature points are set to 900°C, 1100°C and 1300°C. At the same temperature point, the pressure is 500MPa, 1GPa, 1.5GPa, 2GPa, 3GPa and 6GPa. We will use platinum tubes as the vessels for sample packaging, and the samples will be the previously extracted vitrinite, barkinite and inextinite. The recovered platinum capsules will be put into epoxy resin and cut in half: one half will be used for micro-Raman spectroscopy, and the other half will be separated from the platinum capsule, made into powder for X-ray diffraction.

3. Current Research Progress

3.1 Temperature-Controlled Vitrinite Graphitization Kinetic Process

We first conducted vitrification experiments on vitrinite using a piston-cylinder press at a constant pressure of 1 GPa, with annealing times of 10 minutes, 60 minutes, 360 minutes, 720 minutes, and 1440 minutes, at temperatures of 900°C, 1100°C, and 1300°C. The products were then analyzed using X-ray diffraction (XRD) and the interlayer spacing d_{002} was calculated. The results are shown in Figure 3.

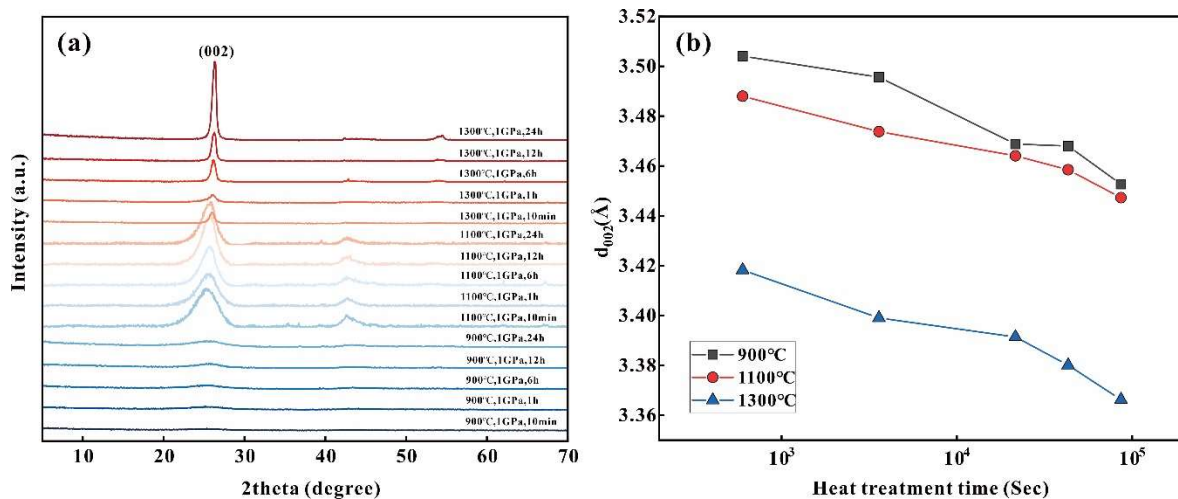


Figure 3. (a) XRD spectra of vitrinite at different temperatures as a function of annealing time. (b)

Variation of d_{002} calculated from XRD spectra as a function of annealing time.

As seen, with increasing temperature and reaction time, the d_{002} peak of vitrinite gradually strengthened and sharpened, and the calculated d_{002} value decreased, indicating an increase in the degree of graphitization. This suggests that the crystallinity of the sample is directly related to the treatment time and temperature. Therefore,

we used power law models (Murty et al., 1969) and Johnson-Mehl-Avrami (JMA) models (Sung, 2000; Khawam and Flanagan, 2006). Prior to applying these kinetic models, we transformed the experimental data into graphitization degree (g) using the following equation:

$$g = (d_0 - d_1)/(d_0 - d_f) \quad (1)$$

Where d_0 is the initial d_{002} spacing value (Figure 3), d_1 is the observed experimental data, and d_f represents the final value of d_{002} spacing (Figure 3). The power law model is one of the most robust kinetic models for carbonization and is widely applied in extrapolating the geological time-temperature range using rate constants and pre-exponential factors. After transforming into dimensionless parameters, we fit the following power law models:

$$g = k_p t^{-n} \quad (2)$$

Where k_p is the rate constant, t is time (s), and n is the reaction order at the given temperature. The experimental data fitted to this equation can provide the rate constant k_p and reaction order n . We then used the following equation to fit the Arrhenius relationship:

$$k_p = A \exp(-E_a/RT) \quad (3)$$

Where k_p is the rate constant, A is the pre-exponential factor, E_a is the effective activation energy, R is the gas constant, and T is the absolute temperature of the experiment. Using the Arrhenius equation, we calculated the effective activation energy to be 148.96 ± 9.29 kJ/mol and demonstrated a good square correlation coefficient of 0.992 (Figure 4b). We also attempted to fit the best fit using the JMA model to describe the complex transformation from amorphous structure to graphite structure (Figure 3). The JMA equation is applicable for heterogeneous nucleation and recrystallization. The equation is represented as:

$$g = 1 - \exp(-k_a t^\ell) \quad (4)$$

Where k_a is the rate constant in the JMA equation, ℓ is the reaction order known as the "Avrami index," and t is the heating duration (s). Taking the natural logarithm of the equation, it can also be written as:

$$\ln[-\ln(1 - g)] = \ln k_a + \ell \ln t \quad (5)$$

By plotting the left-hand side of the equation $\ln[-\ln(1-g)]$ against the natural logarithm of time $\ln t$, the rate constant k_a and Avrami index ℓ can be estimated from the linear regression of the intercept and slope in the Avrami plot. Using the $\ln k_a$ values against $1/T$, we obtained an effective activation energy of 143.67 ± 4.24 kJ/mol and 273 ± 47 kJ/mol for Vitrinite (Figure 4d). Both models described the experimental structural changes during the graphitization of Vitrinite well.

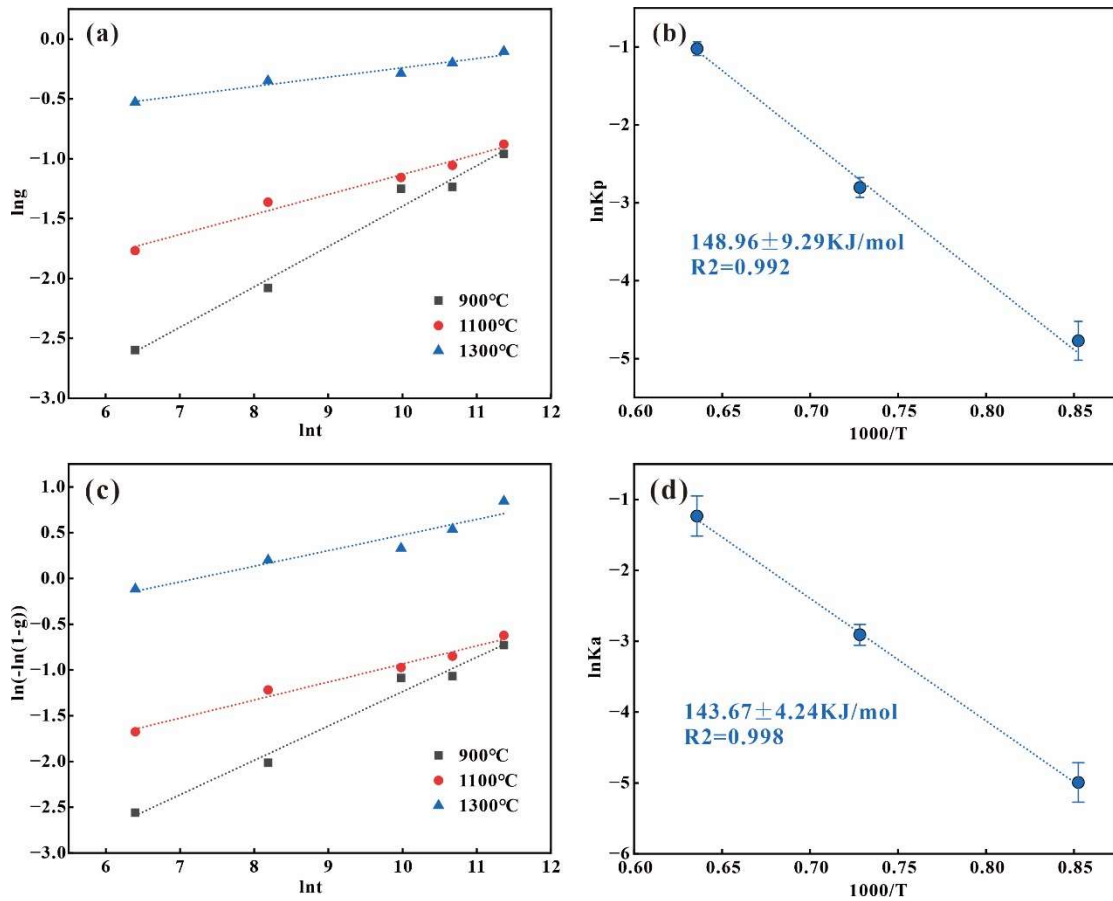


Figure 4. (a) Relationship between $\ln t$ (s) and $\ln g$ for vitrinite fitted by a power law rate model. (c) Also shown is the relationship between $\ln t$ (s) and $\ln[-\ln(1-g)]$ for vitrinite fitted by a JMAK model. (b) & (d) Arrhenius plot of vitrinite.

3.2 Pressure-Controlled Vitrinite Graphitization Kinetic Process

After obtaining the activation energy for Vitrinite at 1 GPa, we further investigated the pressure-controlled graphitization kinetics of Vitrinite. Graphitization experiments were conducted at a constant temperature of 1100°C using both a piston-cylinder press and a multi-anvil press. The annealing times were 10 minutes, 60 minutes, 360 minutes, 720 minutes, and 1440 minutes, and the experiments were performed at pressures of 0.5GPa, 1GPa, 1.5GPa, 2GPa, 3GPa, and 6GPa. The products were analyzed using X-ray diffraction (XRD), and the interlayer spacing (d_{002}) was calculated. The results, as shown in the figure, indicated that as pressure increased, the degree of graphitization of Vitrinite improved, with sharper and more intense d_{002} peaks, suggesting enhanced crystallinity at higher pressures.

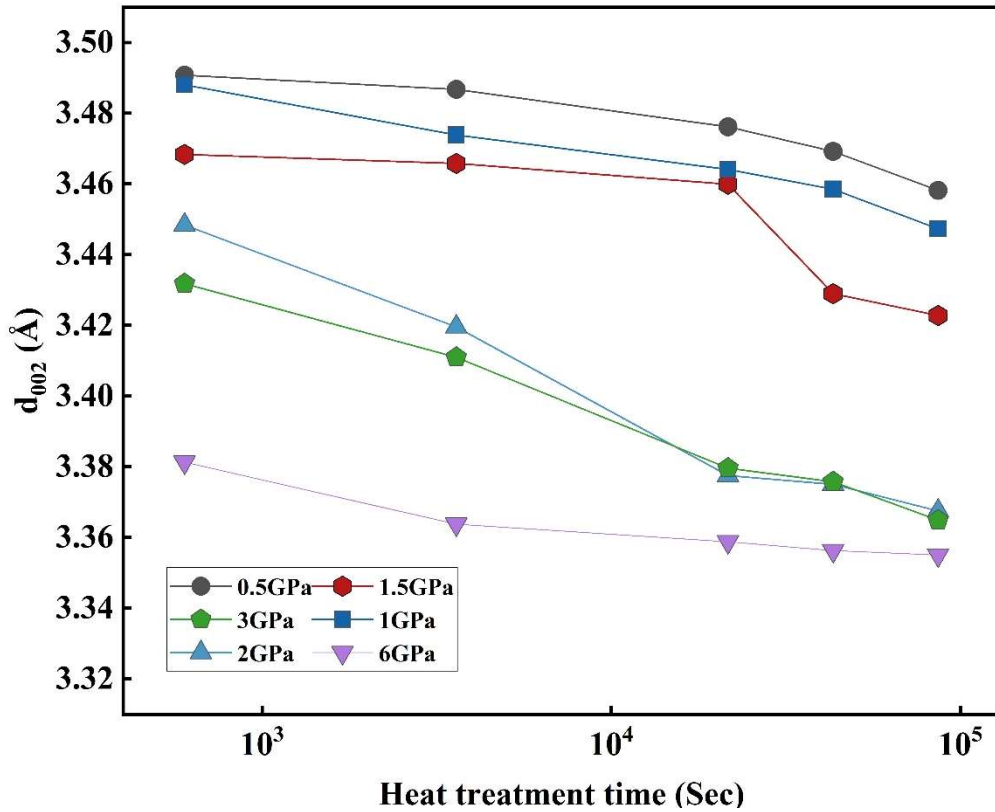


Figure 5. A graph showing the variation of d_{002} spacing with annealing time at different pressures.

The sample shows significant changes in its crystal structure with increasing annealing time and pressure (Figure 5). Therefore, the time-pressure relationship can be used to calculate the pressure dependence of graphitization. We chose the d_{002} spacing of the sample for kinetic analysis because volume analysis is highly sensitive to changes from an amorphous structure to a graphite structure. We first determined the degree of graphitization (g) by applying Equation 1, and after converting to a dimensionless parameter, we applied the power law models from Equation 2 and the JMA models from Equations 4 and 5. In addition to these two methods, we also used the superposition method in our study of graphitization kinetics. By measuring the crystal parameters (d_{002} spacing) at different pressures and appropriately scaling the logarithmic processing time along the time axis, we can superimpose them. The displacement of this distance is called the time-pressure shift factor α_P , which is expressed as follows:

$$\alpha_P = t_P / t_{ref} \quad (6)$$

where t_{ref} is the reference time at a specific reference pressure, and t_P is the time required at a given pressure to produce the same reaction. The crystal properties of the regression curve obtained through the superposition method are shown in Figure 6a. The experimental reference pressure here is 0.5 GPa (4934.6 atm). For each reference pressure, the fully superimposed curve generated by the shift factor is fitted with a nonlinear regression curve (Hill equation). In principle, the reaction mechanism in kinetic experiments should have the same reaction order for both pressure and temperature dependence, which means the same Hill coefficient, h .

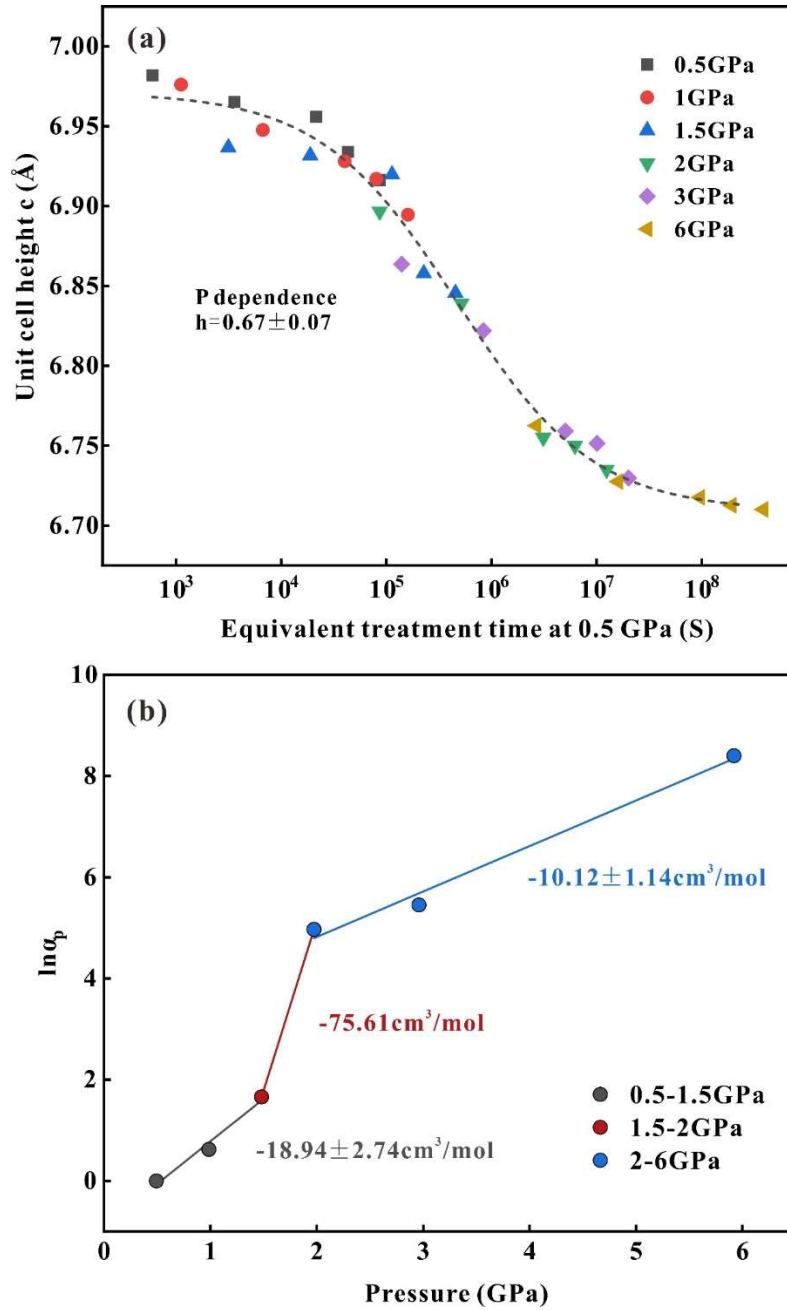


Figure 6. (a) Composite master curves of unit cell height c for vitrinite obtained by shifting the 1.0, 1.5, 2.0, 3.0 and 6.0 GPa curves to combine smoothly with the 0.5 GPa (reference pressure) curve for time–pressure relationships. (b) $\ln \alpha_p$ as functions of pressure were fitted by linear regressions.

We assessed the activation volume of graphitization through logarithmic linear plots of the power law models and JMA models. The pressure dependence in experimental kinetics is described by the activation volume ΔV^\ddagger , which indicates the effect of pressure P on the rate constant k , typically expressed as:

$$\Delta V^\ddagger = -\ln(k_{p,a})RT \quad (7)$$

where P is the pressure (atm), R is the gas constant ($8.314 \text{ J K}^{-1} \text{ mol}^{-1}$), and T is the absolute temperature (K). This equation suggests that if ΔV^\ddagger is independent of pressure, the plot of $\ln(k_{p,a})$ versus P should show a linear relationship, with a slope of $-\Delta V^\ddagger/RT$. However, our experimental results indicate a power law relationship between pressure and the rate constant, suggesting a change in the rate-limiting step at around 1.5 to 2 GPa.

Therefore, the rate constants are fitted with two or three linear approximations (Figure 7b, d). Through the logarithmic linear plot ($\ln(k_{p,a})$ versus pressure), we obtained the activation volumes of the sample within the pressure ranges of 0.5 to 2.0GPa and 2.0 to 6.0GPa as $-19.44 \pm 1.99 \text{ cm}^3/\text{mol}$ and $-4.78 \pm 0.30 \text{ cm}^3/\text{mol}$, respectively. Additionally, within the pressure ranges of 0.5 to 1.5GPa, 1.5 to 2GPa, and 2 to 6.0GPa, the sample's activation volumes are $-16.51 \pm 6.95 \text{ cm}^3/\text{mol}$, $-1.34 \pm 0.01 \text{ cm}^3/\text{mol}$, and $-7.06 \pm 0.35 \text{ cm}^3/\text{mol}$, respectively.

In addition to the power law rate model and JMAK model, another kinetic model (using the superposition method) was applied to determine the pressure effect on graphitization. At a constant temperature (1373 K), the natural logarithm of the time-pressure shift factor, $\ln\alpha_P$, was input into the pressure dependence equation 7. By plotting the relationship between $\ln\alpha_P$ and pressure, this is another method to calculate the ΔV^\ddagger value. The calculated ΔV^\ddagger values and fitted data are shown in Figure 6b. In the pressure range of 0.5 to 1.5GPa, the sample's activation volume is $-18.94 \pm 2.74 \text{ cm}^3/\text{mol}$; in the range of 1.5 to 2.0GPa, it is $-75.61 \text{ cm}^3/\text{mol}$; and in the range of 2.0 to 6.0GPa, it is $-10.12 \pm 1.14 \text{ cm}^3/\text{mol}$. The main curve obtained through the superposition method is fitted with a single S-shaped curve, and the $\ln(\alpha P)$ versus pressure logarithmic linear plot should show a linear relationship. However, our results indicate that the best fit is a power law relationship, not a linear one. This suggests that the continuous reaction of graphitization may not be fully reconstructed by the superimposed main curve of the Hill equation.

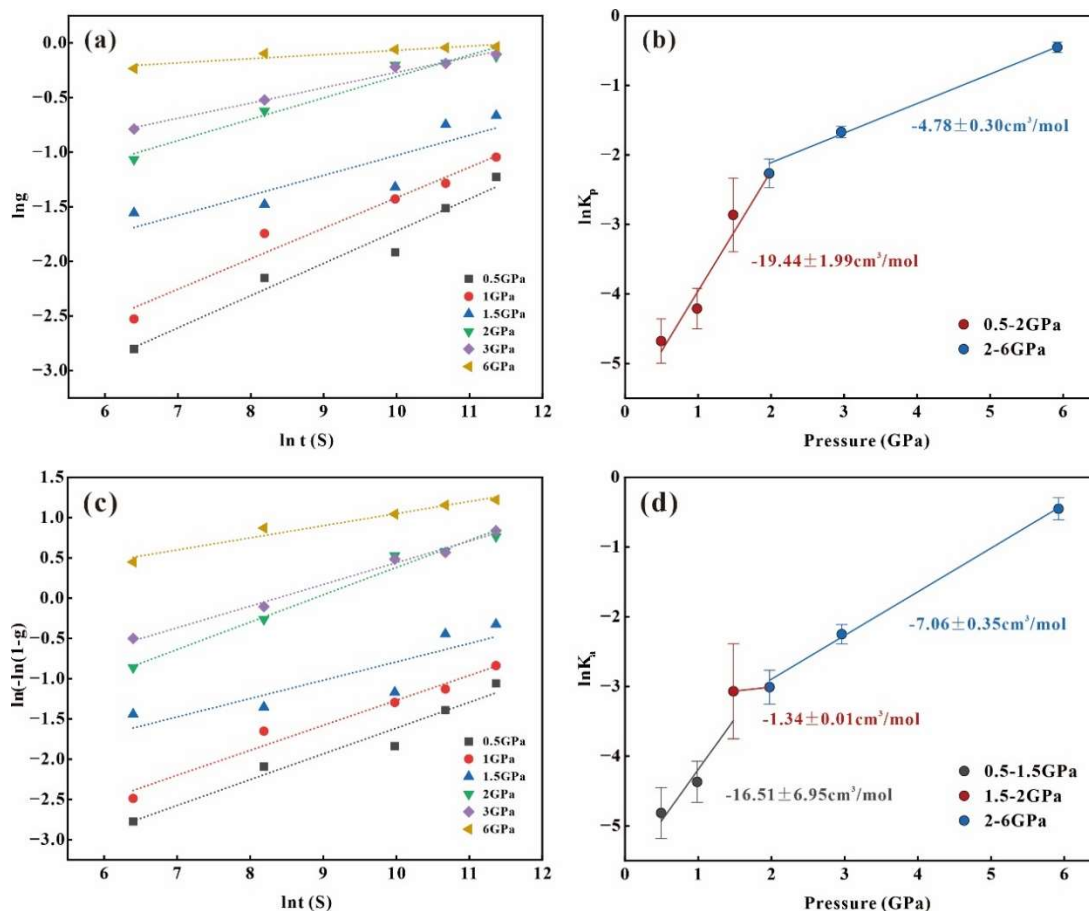


Figure 7. (a) Relationship between $\ln t$ (s) and $\ln g$ for vitrinite fitted by a power law rate model. (c) Also shown is the relationship between $\ln t$ (s) and $\ln[-\ln(1 - g)]$ for vitrinite fitted by a JMAK model. Log-linear

plots of pressure (GPa) vs. $\ln K_p$ (b) and $\ln K_a$ (d). $\ln K_{p,a}$ as functions of pressure were fitted by linear regressions.

where C_{min} and C_{max} are the minimum and maximum values of the unit lattice height c (Å), A_1 is the pre-exponential factor (s^{-1}), T is the absolute temperature (K), R is the gas constant, h is the Hill coefficient, and ΔH is the activation enthalpy (KJ/mol). Equation 8 combines the Hill equation and the Arrhenius relationship determined from time-temperature experiments. In principle, the activation enthalpy under pressure is strictly represented by the following equation: where C_{min} and C_{max} are the minimum and maximum values of the unit lattice height c (Å), A_1 is the pre-exponential factor (s^{-1}), T is the absolute temperature (K), R is the gas constant, h is the Hill coefficient, and ΔH is the activation enthalpy (KJ/mol). Equation 8 combines the Hill equation and the Arrhenius relationship determined from time-temperature experiments. In principle, the activation enthalpy under pressure is strictly represented by the following equation:

$$\Delta H = \Delta E_a + P\Delta V^\ddagger \quad (8)$$

where ΔH is the activation enthalpy, ΔE_a is the activation energy at 1 atm, P is pressure, and ΔV^\ddagger is the activation volume. By combining the Hill equation and Equation 8, we derived the pressure-temperature-time dependence from the sigmoidal main curve (Hill equation) as follows:

$$f(P, T, t) = C_{min} + \frac{C_{max} - C_{min}}{\{1 + [A_1 \exp(-\Delta E_a + P\Delta V^\ddagger / RT) / t]^h\}} \quad (9)$$

By differentiating the power law relationship between $\ln \alpha_p$ and pressure, we calculated the activation volume at each pressure (Figure 8). After differentiation, we converted the activation volume from cm^3/mol to KJ/mol and recalculated the effective activation energy based on the pressure dependence ($P\Delta V^\ddagger$) (Figure 8). On this basis, our geological extrapolation allows the prediction of the structural evolution of deposited organic matter into graphite.

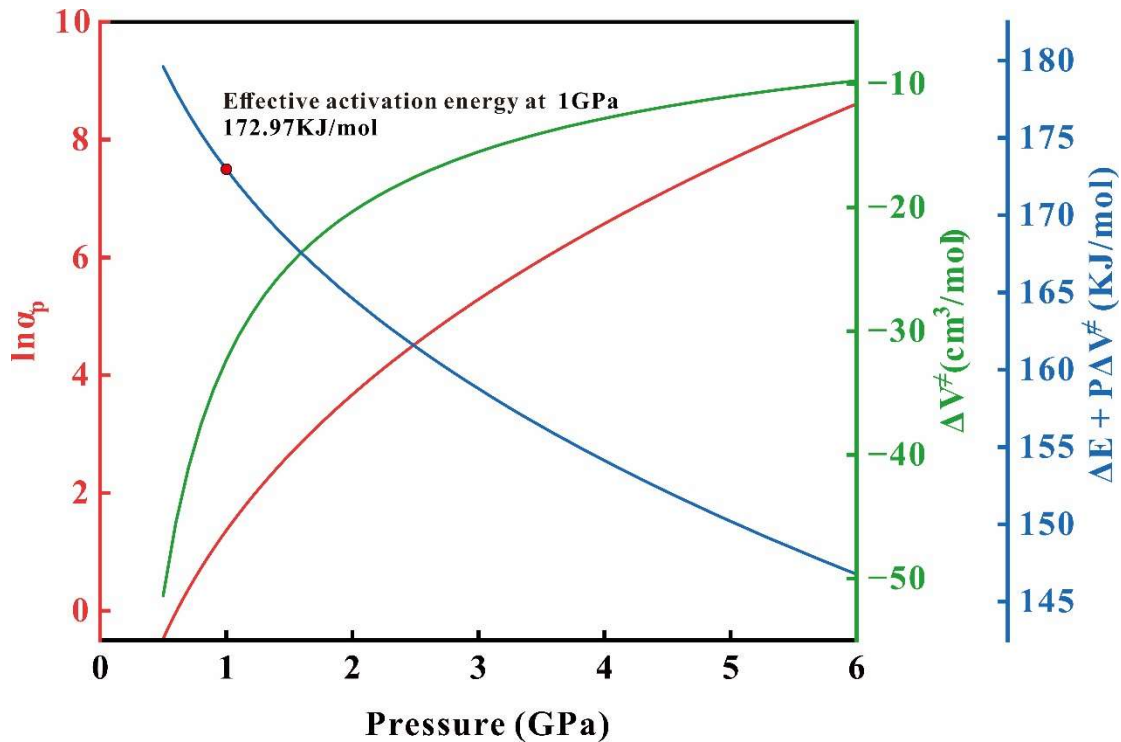


Figure 8. Calculated activation volumes (ΔV^\ddagger) and effective activation energies corrected by pressure dependence ($\Delta E + P\Delta V^\ddagger$) between 0.5 and 6.0 GPa using a superposition method.

Reference

- Atul S., Takashi K., Akira T., 2000. Direct Observation of Layered Structure of Coals by a Transmission Electron Microscope. *Energy & Fuels*. 14, 515-516.
- Beysac O., Goffé B., Chopin C., Rouzaud, J.N., 2002. Raman spectra of carbonaceous material in metasediments: a new geothermometer. *Journal of Metamorphic Geology*. 20, 859–871.
- Beysac O., Rouzaud J.N., Goffé B., Brunet F., Chopin C., 2002. Graphitization in a high-pressure, low-temperature metamorphic gradient: a Raman microspectroscopy and HRTEM study. *Contributions to Mineralogy & Petrology*. 143, 19-31.
- Bonijoly M., Oberlin M., Oberlin A., 1982. A possible mechanism for natural graphite formation. *International Journal of Coal Geology*. 1, 283-312.
- Buseck P.R., Beysac O., 2014. From Organic Matter to Graphite: Graphitization. *Elements*. 10, 421–426.
- Buseck P.R., Tsipursky S.J., Hettich R., 1992. Fullerenes from the geological environment. *Science*. 257, 215-217.
- Bustin R.M., Ross J.V., Rouzaud J.N., 1995. Mechanisms of graphite formation from kerogen: experimental evidence. *International Journal of Coal Geology*. 28, 1-36.
- Bustin R.M., Rouzaud J.N., Ross J.V., 1995. Natural graphitization of anthracite: Experimental considerations. *Carbon*. 33, 679–691.
- Cao Daiyong, Wang Lu, Liu Zhifei, 2020. The research status and prospect of coal-based graphite in China. *Coal Geology & Exploration*. 48, 1-11.
- Cao Daiyong, Zhang He, Dong Jiexiao, 2017. Present situation and key directions of geological research on graphite minerals in coal measures. *Earth Science Frontiers*. 24, 317-327.
- Fischbach D.B., 1963. Kinetics of graphitization of a petroleum coke. *Nature*. 200, 1281–1283.
- Fischbach D.B., 1963. Kinetics of graphitization of a petroleum coke. *Nature*. 200, 1281–1283.
- Fischbach D.B., 1971. The kinetics and mechanism of graphitization. In P.L. Walker, Ed., *Chemistry and Physics of Carbon*. 7, p. 1–154.
- Huang Difan, Qin Kuangzong, Wang Tieguan, 1995. Formation and hydrocarbon generation mechanism of coal-formed oil. Beijing: Petroleum Industry Press.
- Inagaki M., Murase Y., Noda T., 1968. Effect of pre-heat-treatment on kinetics of graphitization. *Journal of the Ceramic Association, Japan*. 76, 184–189
- Jiang Bo, Li Ming, Qu Zhenghui, 2016. Current Research Status and Prospect of Tectonically Deformed Coal. *Advanced Earth Science*. 31, 335-346.
- Kanter M.A., 1957. Diffusion of carbon atoms in natural graphite crystals. *Physical Review*, 107, 655–663.
- Kaxiras E., Pandey K., 1988. Energetics of defects and diffusion mechanisms in graphite. *Physical Review Letters*. 61, 2693–2696.
- Khawam A., Flanagan D.R., 2006. Solid-state kinetic models: Basics and mathematical fundamentals. *The Journal*

of Physical Chemistry B. 110, 17315–17328.

Kouketsu Y., Mizukami T., Mori H., Endo S., Aoya M., Hara H., Nakamura D., Wallis S., 2014. A new approach to develop the Raman carbonaceous material geothermometer for low-grade metamorphism using peak width. *Island Arc*. 23, 33–50.

Liu Zhifei, 2021. The mechanism of graphitization difference of coal macerals based on simulation experiments. Beijing, China University of Mining & Technology, Beijing.

Murty H.N., Biederman D.L., Heintz E.A., 1969. Kinetics of Graphitization—I. Activation energies. *Carbon*, 7, 667–681.

Murty H.N., Biederman D.L., Heintz E.A., 1969. Kinetics of Graphitization—I. Activation energies. *Carbon*, 7, 667–681.

Nover G., Stoll J.B., Jutta von der Gna, 2005. Promotion of graphite formation by tectonic stress—a laboratory experiment. *Geophysical Journal International*. 160, 1059-1067.

Oberlin A., 1984. Carbonization and graphitization. *Carbon*. 22, 521-541.

Oberlin A., Bonnamy S., Oshida K., 2006. Landmarks for graphitization. *TANSO*. 2006, 281–298.

Rantitsch G., Grogger W., Teichert C., Ebner F., Hofer C., Maurer E.M., Schaffer B., Toth M., 2004. Conversion of carbonaceous material to graphite within the Greywacke Zone of the Eastern Alps. *International Journal of Earth Sciences*. 93, 959-973

Ross J.V, Bustin R.M., 1990. The role of strain energy in creep graphitization of anthracite. *Nature*. 343, 58.

Suchy V., Frey M., Wolf M., 1997, Vitrinite reflectance and shear-induced graphitization in orogenic belts: A case study from the Kandersteg area, Helvetic Alps, Switzerland, *International Journal of Coal Geology*. 34, 1-20.

Sung J., 2000. Graphite - diamond transition under high pressure: A kinetics approach, *Journal of Materials Science*. 35, 6041-6054.

Tissot B.P., Welt D.H., 1980. *Petroleum Formation and Occurrence*. Springer-Verlag Berlin Heidelberg New York.

Wilks K.R., Mastalerz M., Bustin R.M., Ross J.V., 1993, The role of shear strain in the graphitization of a high-volatile bituminous and an anthracitic coal. *International Journal of Coal Geology*. 22, 247-277.

Wilks K.R., Mastalerz M., Ross J.V., Bustin R.M., 1993. The effect of experimental deformation on the graphitization of Pennsylvania anthracite. *International Journal of Coal Geology*. 24, 347-369.

Yao Suping, Zhang Jingrong, Jin Kuili, 1996. Study on thermal evolution of macerals by micro fluorescence and micro fourier transform infrared spectroscopy. *Acta Sedimentologica Sinica*. 3, 3-12.

Yilin Chen, Yong Qin, Jiuqing Li, Zhuangfu Li, Tianyu Yang, Ergang Lian, 2022. Discovery of the largest natural carbon onions on Earth, *Science China (Earth Sciences)*. 65, 1736-1750.

Yoshihiro Nakamura, Takashi Yoshino, Madhusoodhan Satish-Kumar, 2017. An experimental kinetic study on the structural evolution of natural carbonaceous material to graphite. *American Mineralogist*. 102, 135-148.

Yoshihiro Nakamura, Takashi Yoshino, Madhusoodhan Satish-Kumar, 2020. Pressure dependence of graphitization: implications for rapid recrystallization of carbonaceous material in a subduction zone.

Contributions to Mineralogy & Petrology. 175, 1-14.